Modeling contact electrification in triboelectric impact oscillators as energy harvesters

Hongcheng Tao[a], Gregory Batt[b], and James Gibert[a]

[a]Purdue University, 610 Purdue Mall, West Lafayette, USA
[b]Clemson University, Clemson, USA

ABSTRACT

Triboelectric energy harvesters or nanogenerators exploit both contact electrification and electrostatic induction to scavenge excess energy from random motions of mechanical structures. This study focuses on the modeling of triboelectric energy harvesters in the configuration of contact-separation impact oscillators. While mechanical and electrostatic elements in such systems can be satisfactorily modeled based on existing theories, the underlying physics of contact electrification is still under debate. The aim of this work is to introduce the surface charge density of dielectric layers as a variable into the macroscopic equations of motion of triboelectric impact oscillators by experimentally investigating the relation between the impact force and the charge transfer during contact electrification. Specifically, specimens with selected pairs of materials are put under a solenoid-driven pressing tester which charges the specimens with a vertical force whose magnitude, frequency and duty cycle can be controlled. An electrometer is used to monitor the short circuit charge flow between the electrodes from which the charge accumulation on dielectric layers can be extracted. With results from parameter-sweep tests, the produced map from contact force to surface charge density can be integrated into equations of motion via curve fitting or interpolation.

Keywords: Triboelectric nanogenerator, energy harvester, contact electrification, electrostatic induction, impact oscillator

1. INTRODUCTION

Triboelectric nanogenerators (TENGs), utilizing a combination of contact electrification and electrostatic induction, have been widely studied in recent years with applications such as mechanical energy harvesters[1–7] and self-powering sensors.[8–11] Numerous efforts have been paid to model the dynamics of TENGs where fundamental electrostatic theories have been established that satisfactorily match experimental results. Among various configurations, the contact-separation-type TENGs are most frequently investigated due to the simplicity of their structure which consists of only one or two dielectric layers adhered to electrodes.[1,12–15] In most analyses on this type of TENGs, focus is maintained on the steady-state performance assuming that the charge distributed on triboelectric surfaces has reached saturation and is constant throughout. Under this assumption, simplified electrostatic models taking the triboelectric surfaces as infinite parallel planes have been used to predict the output characteristics of the TENGs.[15] At the same time, a more realistic model that includes the distance dependence of electric field strengths has been reported to fit experimental data better.[16] However, this assumption of constant surface charge may not be sufficient to reflect practical cases. On one hand, saturated triboelectric surfaces may be subject to fluctuating ambient environment including temperature[17] and humidity that may cause charge dissipation.[18] On the other hand, it is desired that the surface charge accumulation should result directly from contact electrification during the operation of TENGs so that no preparatory charging is required. Moreover, since the amount of charge transfer is related to the true contact area between the triboelectric surfaces and thus dependent on the contact force, especially for TENGs with irregular surface topographies the surface charge densities at saturation may differ distinctly according to the practical operating conditions.

Further author information: (Send correspondence to Hongcheng Tao)
Hongcheng Tao: E-mail: taoh@purdue.edu, Telephone: 1 765 775 0948
James Gibert: E-mail: jgibert@purdue.edu
Gregory Batt: E-mail: gbatt@clemson.edu

Nonetheless, the significance of modeling contact electrification for contact-separation TENGs is tricky to define. Since the charging through contact electrification usually follows an exponential trend,[19,20] modeling them thus as an asymptotic process in fact differs very little from the classical models assuming constant surface charge densities considering steady-state performances. Therefore in this paper, although an exponential charge accumulation is also observed in experiments, this transient effect is not emphasized and instead focus is placed on the saturated value's dependence on the steady-state motion of the oscillator. Briefly, the surface charge densities on dielectric layers appear in a quasi-dynamic way in that while they are constant during steady-state operation of the TENG, this constant value is dependent on the intensity of the impacts, or in other words, the contact force between the triboelectric layers in steady state. In what follows, the experimental procedures applied to determine such dependence will be introduced, featuring the theoretical background of the method adopted for monitoring the charge transfer during contact electrification.

2. METHODOLOGY

In this section the problem statement will be first given with respect to the role played by the dielectric surface charge densities in the classical equations of motion for contact-separation triboelectric impact oscillators. Then an experimental method will be illustrated that can approximately monitor the transient charge transfer to the dielectric layers. Employing this method, test procedures will be introduced for examining the relation between the charge accumulation at saturation and the magnitude of the contact force.

2.1 The Classical Contact-Separation TENG Model

A classical contact-separation TENG contains two motion parts, as shown in Fig 1 (neglecting the connection in dashed wires), where a dielectric layer with thickness d_1 and an electrode adhered to its back, referred to as the electrostatic electrode, constitute the first (upper) part. In the single-dielectric configuration, the second part consists of simply another electrode, named as the contact electrode, which is placed at a distance $d_2 + x$ away from the first part, where d_2 is some fixed constant and x is the displacement variable. In the double-dielectric configuration, the second part is instead composed of another dielectric layer with an electrode on its back. In both configurations when the two parts come into contact, electrification happens so that charge is transfered between the contacting surfaces and remains on them after separation. Then when x varies, the electric field formed by the surface charge on the dielectric layer(s), whose densities are labeled as σ_d and σ_b, will induce a varying potential between the electrodes so that charge will flow from one to the other if they are short circuited or connected to an external load, performing like an AC power source. Utilizing such mechanism, an energy harvester can then be built by assigning inertial (mass) and stiffness components to the two parts to form an impact oscillator. Suppose that the first part is modeled as a rigid body with mass m and connected to the second part with a linear spring of stiffness k, and further suppose d_2 is then defined as the gap distance at equilibrium. Let the second part be fixed on some main structure from which excess kinetic energy is to be harvested, which is equivalent to applying a base excitation to the first part. Furthermore, describe the impacts between the two parts with a Hertzian contact model. Assuming some external load R and neglecting for simplicity the electrostatic forces so that the mechanical motion is independent of the electrostatics, the equations of motion for this constructed triboelectric impact oscillator are then given by

$$\begin{cases} m\ddot{x} + c\dot{x} + kx = F_b(t) + f_c(x) \\ R\dot{\sigma}_e + \left(\dfrac{d_1}{\varepsilon_1 A} + \dfrac{x + d_2}{\varepsilon_2 A}\right)\sigma_e + \dfrac{x + d_2}{\varepsilon_2 A}\sigma_d = 0 \end{cases} \tag{1}$$

for the single-dielectric configuration and

$$\begin{cases} m\ddot{x} + c\dot{x} + kx = F_b(t) + f_c(x) \\ R\dot{\sigma}_e + \left(\dfrac{d_1}{\varepsilon_1 A} + \dfrac{x + d_2}{\varepsilon_2 A} + \dfrac{d_3}{\varepsilon_3 A}\right)\sigma_e + \dfrac{x + d_2}{\varepsilon_2 A}\sigma_d = 0 \end{cases} \tag{2}$$

for the double-dielectric configuration, where

$$f_c(x) = \begin{cases} k_c(-x - d_2)^{\frac{3}{2}} & \text{if } x \le -d_2 \\ 0 & \text{if } x > -d_2 \end{cases} \tag{3}$$

describes the piecewise contact force, $F_b(t)$ represents the base excitation, A is the area of the surfaces and ε_1, ε_2 and ε_3 are the permittivities of the first dielectric, air and the second dielectric, respectively.

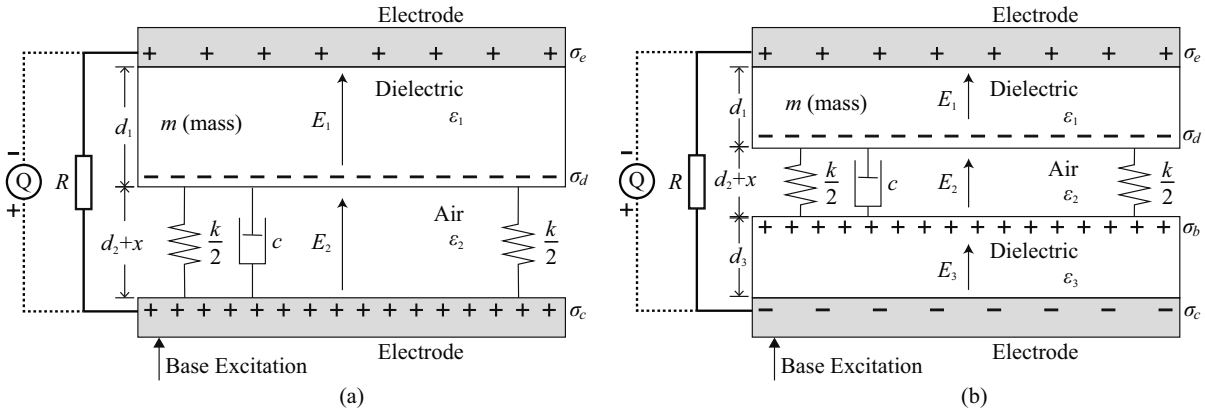

Figure 1. Schematics of the a) single- and b) double-dielectric configurations for contact-separation TENGs assembled into triboelectric impact oscillators

Consider the operation of such triboelectric impact oscillators under some specific base excitations for energy harvesting. Assume that the surfaces are not charged at rest so that all surface charge densities are initially zero. During the vibrations the surfaces come into contact whose characteristics will determine the amount of charge transfered by electrification, for which the limit case would be that under some critically slight excitations the amplitude of the vibration is so small that no impact and thus no electrification can happen. The following sections will then illustrate the experimental procedures used to quantify such relation between charge transfer and contact force.

2.2 Monitoring Charge Transfer

Real-time monitoring of charge transfer between the contacting surfaces of a triboelectric device has been a challenge for studies in the field. While the direct measurement of surface charge typically requires the disassembly of the device[21–23] which inevitably will add to the sources of error, it is often estimated from the system's output voltage under the infinite-parallel-plane assumption so that the open-circuit voltage can be related to the surface charge densities straightly according to Gauss's law. In this work, we adopted a similar method to estimate the charge transfer via the measurement of short-circuit charge flow. The method is capable of getting around errors caused by uncertainties in system parameter estimations such as the dielectric layer thicknesses and permittivities of the materials.

Consider first the single-dielectric contact-separation TENG configuration shown in Fig. 1a. Neglecting the designed inertial and stiffness components and focusing on the electrostatic system only, assume negligible thicknesses for the electrodes and let them be connected to an electrometer (Keithley Model 6514) in charge measurement mode, as shown in dashed wires in Fig. 1a, so that a short circuit is formed and the electrometer readings indicate the charge flow which equals to $\Delta Q_e = \Delta\sigma_e A$, where σ_e is the surface charge density of the electrostatic electrode. Regarding the surfaces first as infinite parallel planes, the electric field strengths E_1 inside the dielectric and E_2 inside the air gap are

$$E_1 = \frac{\sigma_c + \sigma_d - \sigma_e}{2\varepsilon_1},\ E_2 = \frac{\sigma_c - \sigma_d - \sigma_e}{2\varepsilon_2}\ , \tag{4}$$

where σ_c is the surface charge density of the contact electrode. Define an initial position where $x = 0$ so that at any time instant the short circuit condition requires the output voltage to be zero:

$$V_{sc} = E_1 d_1 + E_2 d_2 = 0\ \Rightarrow\ \left(\frac{d_1}{\varepsilon_1} + \frac{d_2}{\varepsilon_2}\right)(\sigma_c - \sigma_e) + \left(\frac{d_1}{\varepsilon_1} - \frac{d_2}{\varepsilon_2}\right)\sigma_d = 0\ . \tag{5}$$

Suppose that after a certain period of time during which x varies and impacts happen, an amount of charge $\Delta\sigma_d = -(\Delta\sigma_c + \Delta\sigma_e)$ is transfered between the dielectric surface and the contact electrode. Assuming that the surfaces have returned to the initial positions so that again $x = 0$, by Eq. 5 there is

$$\left(\frac{d_1}{\varepsilon_1} + \frac{d_2}{\varepsilon_2}\right)(\Delta\sigma_c - \Delta\sigma_e) + \left(\frac{d_1}{\varepsilon_2} - \frac{d_2}{\varepsilon_2}\right)\Delta\sigma_d = 0 \;\Rightarrow\; \Delta\sigma_d = -\left(1 + \frac{d_1\varepsilon_2}{d_2\varepsilon_1}\right)\Delta\sigma_e \;, \tag{6}$$

where $\Delta\sigma_e$ is directly measured by the electrometer given that the surface area of the electrostatic electrode is known. In this way the real-time charge transfer after any charging duration, as long as the electrodes return to their initial positions, can be directly monitored without the necessity to unmount the specimens so that disturbance caused by measurement operations is minimized. In practice, it is usually valid that $d_2 \gg d_1$ and thus it can be further assumed that $\Delta\sigma_d \approx -\Delta\sigma_e$ so that the measurement directly provides a close estimation for the amount of charge transfer. A similar result for the double-dielectric configuration shown in Fig. 1b is

$$\Delta\sigma_d = -\left(1 + \frac{d_1\varepsilon_2}{d_2\varepsilon_1} + \frac{d_3\varepsilon_2}{d_2\varepsilon_3}\right)\Delta\sigma_e \;, \tag{7}$$

for which it can also be assumed that $\Delta\sigma_d \approx -\Delta\sigma_e$ if $d_2 \gg d_1$ and $d_2 \gg d_3$ are both valid.

It is claimed that the presented method is also applicable in situations where the infinite-parallel-plane assumption is invalid when d_2 is comparably large. Consider in such cases the electric field strengths are distance-dependent so that for a rectangular surface with length l, width w and surface charge σ the surrounding electric field strength in a dielectric with permittivity ε at a distance z away from the surface is[16]

$$|E(z)| = \frac{\sigma}{\pi\varepsilon}\arctan\frac{wl}{2z\sqrt{4z^2 + w^2 + l^2}} \triangleq \frac{\sigma}{\varepsilon}f(z) \;. \tag{8}$$

The short-circuit condition and the assumption of charge conservation yield

$$\frac{\Delta\sigma_d}{\Delta\sigma_e} = -\frac{\varepsilon_2\int_0^{d_1}[f(z+d_2) + f(d_1 - z)]\mathrm{d}z + \varepsilon_1\int_0^{d_2}[f(z) + f(d_1 + d_2 - z)]\mathrm{d}z}{\varepsilon_2\int_0^{d_1}[f(z+d_2) - f(z)]\mathrm{d}z + \varepsilon_1\int_0^{d_2}[f(z) + f(d_2 - z)]\mathrm{d}z} \tag{9}$$

for the single-dielectric configuration, and for the double-dielectric configuration there is

$$\frac{\Delta\sigma_d}{\Delta\sigma_e} = -\frac{I_1 + I_2 + I_3}{I_4 + I_5 + I_6} \;, \tag{10}$$

where

$$\begin{cases} I_1 = \varepsilon_2\varepsilon_3\displaystyle\int_0^{d_1}[f(z+d_2+d_3) + f(d_1 - z)]\mathrm{d}z \\ I_2 = \varepsilon_1\varepsilon_3\displaystyle\int_0^{d_2}[f(z+d_3) + f(d_1+d_2 - z)]\mathrm{d}z \\ I_3 = \varepsilon_1\varepsilon_2\displaystyle\int_0^{d_3}[f(z) + f(d_1+d_2+d_3 - z)]\mathrm{d}z \end{cases}, \quad \begin{cases} I_4 = \varepsilon_2\varepsilon_3\displaystyle\int_0^{d_1}[f(z+d_2) - f(z)]\mathrm{d}z \\ I_5 = \varepsilon_1\varepsilon_3\displaystyle\int_0^{d_2}[f(z) + f(d_2 - z)]\mathrm{d}z \\ I_6 = \varepsilon_1\varepsilon_2\displaystyle\int_0^{d_3}[f(d_2+d_3 - z) - f(d_3 - z)]\mathrm{d}z \end{cases} . \tag{11}$$

The integrals are then evaluated under the following test conditions to briefly verify the validity of estimating $\Delta\sigma_d$ with $\Delta\sigma_e$. In experiments for the single-dielectric configuration, PTFE tape (3M 5490) is used as the dielectric layer while copper is used as the electrostatic electrode and ITO(Indium Tin Oxide)-coated PET film (Sigma-Aldrich 639303) as the contact electrode. In the double-dielectric configuration, the same PTFE-copper combination is used as one dielectric and a nylon-copper combination is used as the other where nylon films are prepared on a 3d printer. All layers are cut into rectangles for which $l \approx 45$mm and $w \approx 35$mm. The system parameters are listed in Table 1.

The numerically evaluated integrals in Equations 9 and 10 under the listed parameters and the relations between $\dfrac{\Delta\sigma_d}{\Delta\sigma_e}$ and the gap distance d_2 at the initial position are depicted in Fig. 2. It is indicated that at $d_2 = 4.3$mm, which is the designated air gap clearance at rest for all following tests, the difference between the electrometer reading $|\Delta\sigma_e|$ and the charge accumulation on the dielectric surface $|\Delta\sigma_d|$ is less than 2% for both single- and double-dielectric configurations.

Table 1. System Configurations

Single-Dielectric Configuration

Part	Material	Rel. Permittivity	Thickness
Dielectric	PTFE	$\varepsilon_1 = 2.1$	$d_1 = 0.09$ (mm)
Air	Air	$\varepsilon_2 = 1.0$	$d_2 = 4.3$ (mm) $(x = 0)$
Contact Electrode	ITO	\	\
Electrostatic Electrode	Copper	\	\

Double-Dielectric Configuration

Part	Material	Rel. Permittivity	Thickness
Dielectric 1	PTFE	$\varepsilon_1 = 2.1$	$d_1 = 0.09$ (mm)
Air	Air	$\varepsilon_2 = 1.0$	$d_2 = 4.3$ (mm) $(x = 0)$
Dielectric 2	Nylon	$\varepsilon_3 = 4.5$	$d_3 = 0.13$ (mm)
Electrodes	Copper	\	\

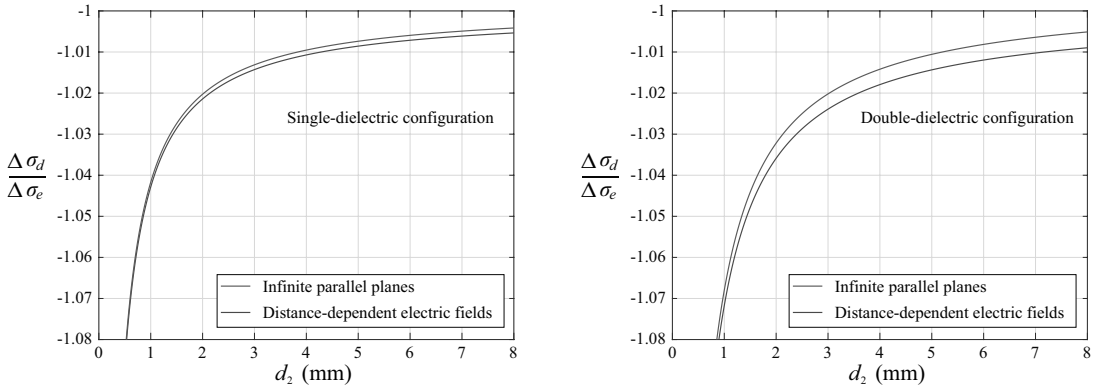

Figure 2. Variation of $\frac{\Delta\sigma_d}{\Delta\sigma_e}$ with d_2 under infinite-parallel-plate and distance-dependent-electric-field assumptions

2.3 Experiment Setup

Employing the method for charge transfer estimation introduced above, specimens configured as listed in Table 1 are tested with a home-built solenoid-based pressing tester shown in Fig 3. The tester drives the contact-separation motion of the specimens while exerting contact forces with controlled magnitude (measured by a bar load cell), frequency and duty cycle. When at rest, the specimens are kept at a distance $d_2 = 4.3$mm away from each other. The electrometer monitors the charge flow between the electrodes so that when the surfaces come back to the initial position after a certain number of contact-separation motion cycles, the electrometer readings give an approximation of the charge transfer to the dielectric layer(s).

Before each run, the surfaces are cleaned with isopropyl alcohol and deionized water successively so that the surface charge accumulated in previous runs is dissipated. During each run, the specimen undergoes a periodic compressing force with a constant magnitude at 1 Hz with a 50% duty cycle (so that each cycle includes 0.5s of contact and 0.5s of separation). The measured charge (density) flow $\Delta\sigma_e$ is recorded for the first 1000 seconds of charging.

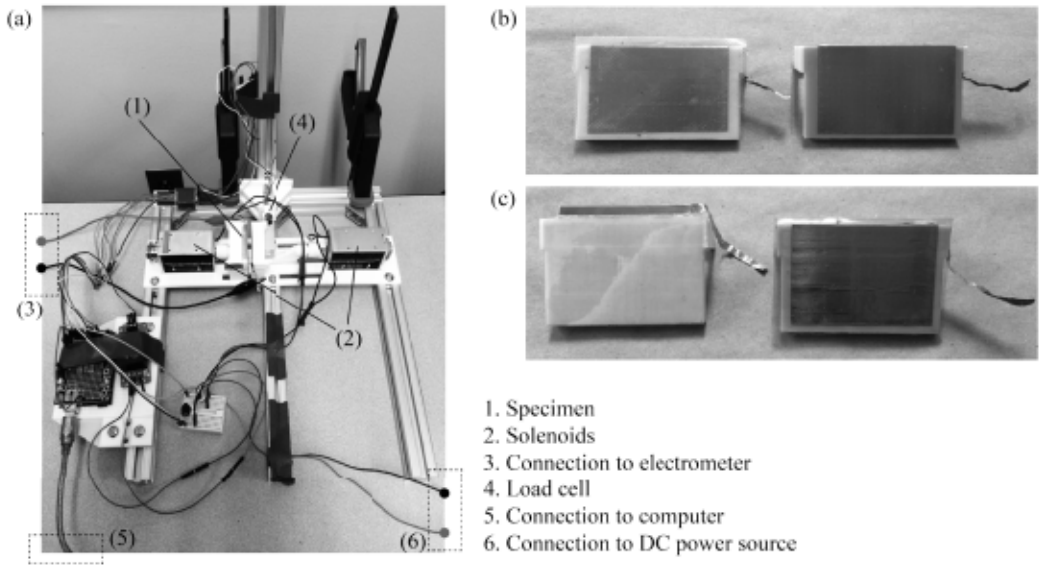

Figure 3. The experiment apparatus: a) a solenoid-based pressing tester; b) a double-dielectric PTFE-nylon specimen; c) a single-dielectric PTFE-ITO specimen

3. RESULTS

Employing test procedures described above, the PTFE-nylon and PTFE-ITO specimens are tested separately. In the following a sample test curve will first be depicted, from which a method to extract the charge accumulation history will be demonstrated. Applying this method the relation between the surface charge density at saturation and the magnitude of the contact force is mapped for both specimens via a series of parameter-sweep tests. Based on the experimental results, at last the proposed modifications will be described that integrate this relation into the equations of motion for the triboelectric impact oscillator.

3.1 Relations Between Saturation Charge Density and Contact Force

A typical response curve for the double-dielectric (PTFE-nylon) TENG is depicted in Fig. 4 under a constant force magnitude of 10N. The response curve appears in a square wave manner where the peak values represent measurements when the surfaces are at the original position $d_2 = 4.3$mm and the valleys represent measurements when they are in contact so that $x \leq -d_2$. As illustrated in Section 2.2, the amount of charge transfer can be monitored by tracking the peak values only, as labeled in red in Fig. 4, which is hereby named the charging curve. In this particular test run, the charge accumulation on the dielectric layers has shown an exponential trend and reached saturation with a surface charge density of $\sim$2.25 μC/m^2 according to the charging curve.

After cleaning, the same specimen is then tested under identical conditions except with different force magnitudes. The charging curves are extracted from the response curves and Fig. 5a demonstrates for each force magnitude a selected charging curve. Despite the observed fluctuations, the surface charge density at saturation has shown a clear dependence on the force magnitude. In order to quantify such relation the average surface charge density within time range 500s to 1000s, regarded as saturated, is again averaged among different runs for each force magnitude. As the result, Fig 5b shows the map for such dependence which appears in a linear manner within the range of the examined force magnitudes. Results for the PTFE-ITO specimen are shown in a similar way in Fig. 6 where the charging curves show richer transient behaviors under large contact forces and the charge-force dependence appears more irregular.

3.2 Force-Dependent Short Circuit Charge Flow

The previous section (3.1) has provided an applicable scheme to model the dielectric surface charge densities at saturation given information of contact forces during the steady-state operation of triboelectric impact oscillators

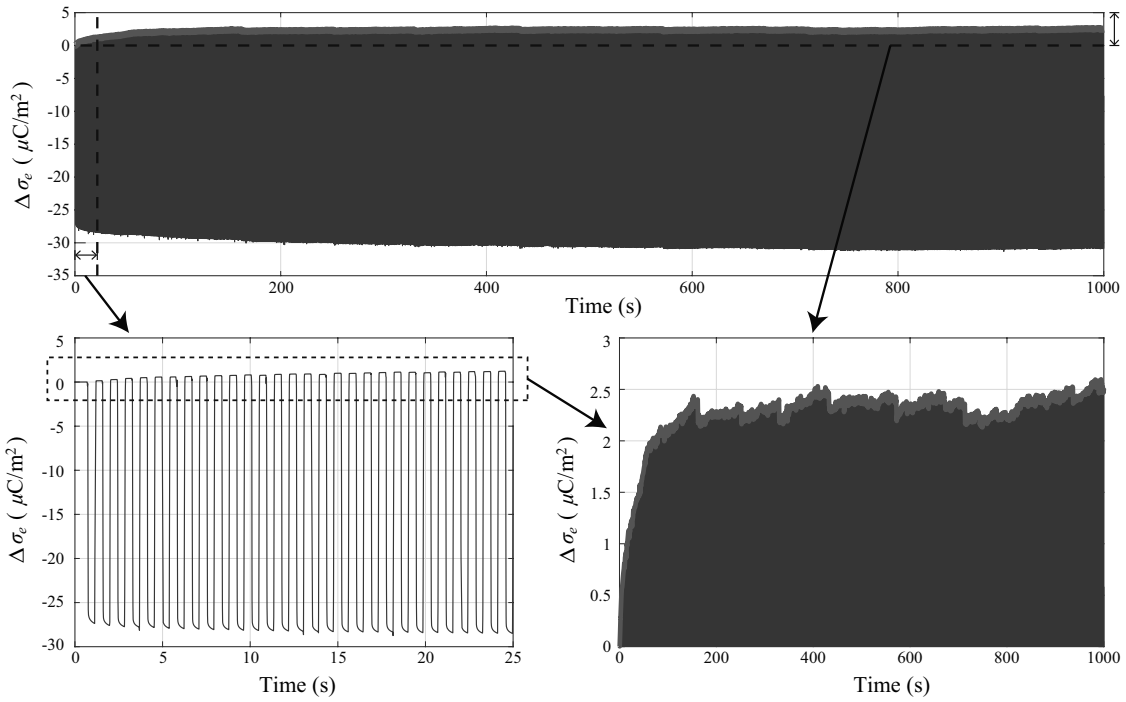

Figure 4. A sample short-circuit charge flow curve of double-dielectric PTFE-nylon specimen under pressing force with constant magnitude 10N at 1Hz with 50% duty cycle, where the contour in red represents the charging curve

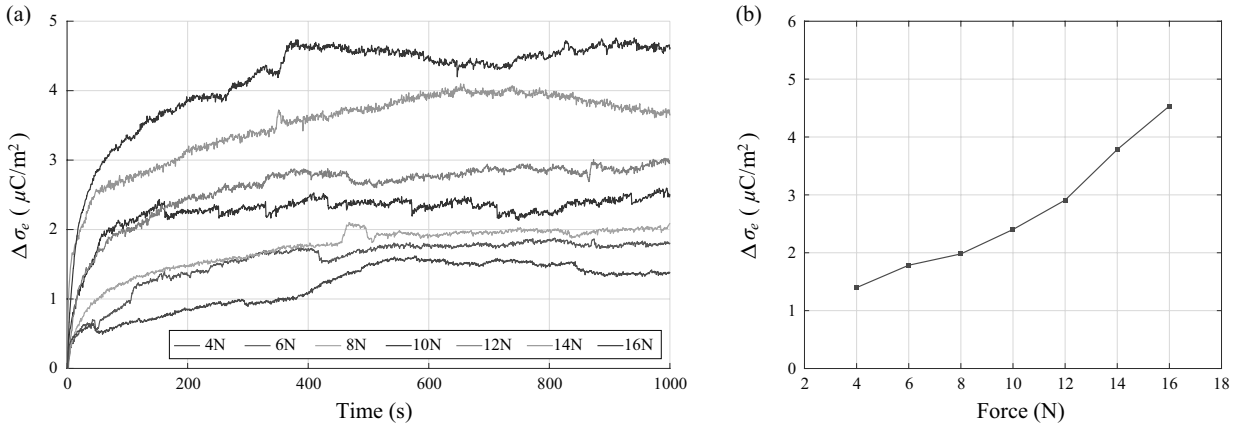

Figure 5. Force dependence of the contact electrification of a PTFE-nylon interface: a) charging curves under a pressing force at 1Hz with 50% duty cycle and different magnitudes; b) relation between surface charge density at saturation and the force magnitude

/ contact-separation TENGs. This model is sufficient for predicting the output characteristics during motions of the devices when the surfaces are separated, i.e., $x > -d_2$. However, experimental results have shown that a significant portion of the short circuit charge flow is induced when the surfaces are in contact so that $x \leq -d_2$. This is partially because the prepared surfaces are not perfectly flat, which is also true for all practical situations, so that the surface asperities allow considerable clearances when their tips first come into contact. With an increasing contact force the asperities are compressed, reducing the clearances so that more charge flow is induced. This effect is significant since although the clearances caused by irregular surface topography is small compared to the stroke of motion when the surfaces are separated, the electrostatic induction is exponentially stronger when

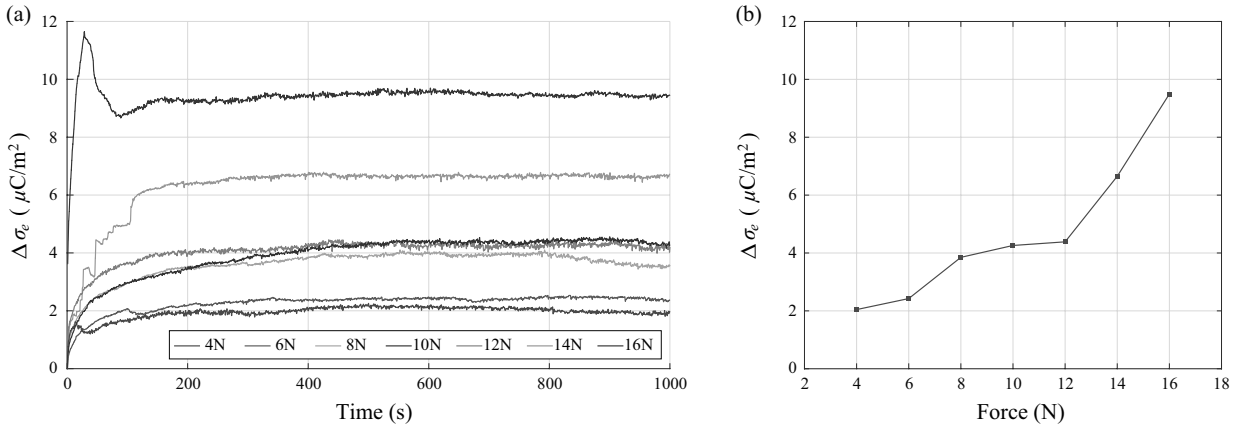

Figure 6. Force dependence of the contact electrification of a PTFE-ITO interface: a) charging curves under a pressing force at 1Hz with 50% duty cycle and different magnitudes; b) relation between surface charge density at saturation and the force magnitude

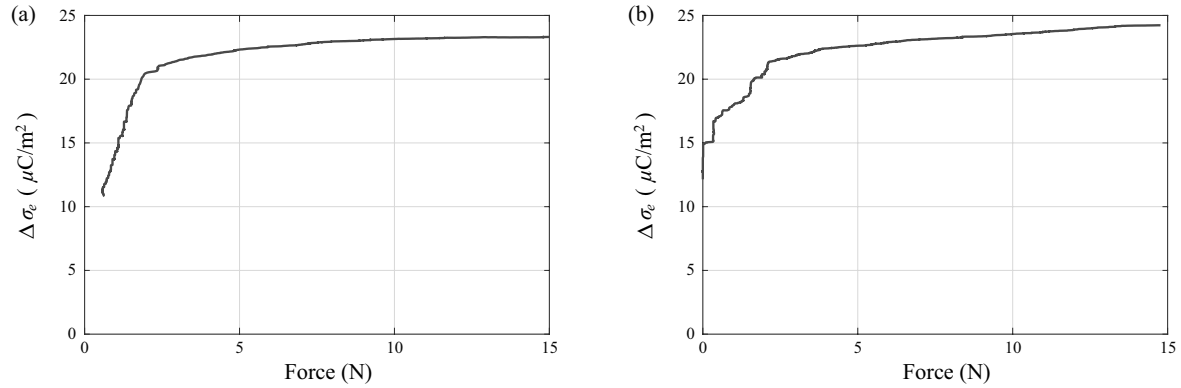

Figure 7. Charge flow between electrodes of the a) PTFE-nylon and b) PTFE-ITO specimens with increasing contact force after charged to saturation under a cyclic 16N force

the surfaces are getting closer. Therefore, it is claimed in this work that the contact force magnitude should not only affect the dielectric surface charge densities at saturation (which dominates the system output when the surfaces in motion are separated) but also introduce excess charge flow when the surfaces are in contact. In other words, distance dependence of charge flow during non-rigid contacts is transfered to a force dependence assuming non-smooth surfaces. Using the same experiment apparatus, this part of the model is briefly investigated by first charging a specimen to saturation with a fixed force magnitude of 16N and then applying a quasi-static force on the surfaces in contact to measure the short circuit charge flow. In Fig. 7a the PTFE-nylon specimen is tested and the relation between the change in the electrostatic electrode charge density and the contact force is depicted, where the zero charge flow is defined when the surfaces are separated by $d_2 = 4.3$mm. Limited by the solenoid structure, information at forces near zero is missing but it can be interpreted that the charge (density) flow during the full stroke from $x = 0$ to $x = -d_2$ is no larger than $\sim 10\mu\text{C/m}^2$ and thus the charge flow caused by the contact force, which can be up to two times that during the motion in separation, is not to be neglected. Moreover, the short-circuit charge flow reaches some saturation value with increasing contact force, indicating a nearly complete elimination of microscopic clearances by full compression of the surface asperities. Similar results for the PTFE-ITO specimen are shown in Fig. 7b.

3.3 Proposed Modifications on the TENG Dynamic Model

According to observations presented in Sections 3.1 and 3.2, two modifications are then proposed on the classical equations of motion 1 and 2. The first modification includes the dependence of the saturated dielectric surface charge density on the contact force so that instead of setting σ_d as a constant, it is related to the time history of the contact force $f_c(x)$ within a fixed time constant T by

$$\sigma_d(x(t)) = f_s\left(\sup\left\{f_c(x(\tau)),\, \tau \in [t-T, t]\right\}\right) \ , \tag{12}$$

where f_s is to be fit or interpolated from experimental results for each particular specimen via approaches similar to Section 3.1.

The second modification briefly introduces the excess induced charge flow due to the compression of asperities on the surfaces in contact which can be represented by replacing the electrostatic equations in 1 and 2 with

$$R\dot{\sigma}_e + \left(\frac{d_1}{\varepsilon_1 A} + \frac{x+d_2}{\varepsilon_2 A}\right)\sigma_e + \frac{x+d_2}{\varepsilon_2 A}\sigma_d(x(t)) = f_e'(f_c(x))f_c'(x)\dot{x} = \begin{cases} -\dfrac{3}{2}k_c\dot{x}\sqrt{-x-d_2}f_e'(f_c(x)) & \text{if } x \le -d_2 \\ 0 & \text{if } x > -d_2 \end{cases} \tag{13}$$

and

$$R\dot{\sigma}_e + \left(\frac{d_1}{\varepsilon_1 A} + \frac{x+d_2}{\varepsilon_2 A} + \frac{d_3}{\varepsilon_3 A}\right)\sigma_e + \frac{x+d_2}{\varepsilon_2 A}\sigma_d(x(t)) = \begin{cases} -\dfrac{3}{2}k_c\dot{x}\sqrt{-x-d_2}f_e'(f_c(x)) & \text{if } x \le -d_2 \\ 0 & \text{if } x > -d_2 \end{cases} \tag{14}$$

for the single- and double-dielectric configurations, respectively. Again the function f_e that relates the excess charge flow to contact force is fit from experimental results following Section 3.2.

4. CONCLUSIONS

In this work the influence of contact force on the performance of contact-separation TENGs is investigated. As a complement to the existing models that treat dielectric surface charge densities as constant parameters, it is proposed in this paper that its saturation value is dependent on the contact force in operation and this relation is introduced into the equations of motion of triboelectric impact oscillators. Besides, the excess charge flow between electrodes caused by further compression of surface asperities is also established as a contact force dependent model and integrated into the equations of motion. The proposed model is to be examined by vibration tests on triboelectric impact oscillators in future work.

ACKNOWLEDGMENTS

This work is supported by the National Science Foundation under Grant: CMMI 1662925.

REFERENCES

[1] Wu, C., Wang, A. C., Ding, W., Guo, H., and Wang, Z. L., "Triboelectric nanogenerator: A foundation of the energy for the new era," *Advanced Energy Materials* **9**(1), 1802906 (2019).

[2] Fan, F.-R., Tian, Z.-Q., and Wang, Z. L., "Flexible triboelectric generator," *Nano energy* **1**(2), 328–334 (2012).

[3] Wang, Z. L., "Triboelectric nanogenerators as new energy technology for self-powered systems and as active mechanical and chemical sensors," *ACS nano* **7**(11), 9533–9557 (2013).

[4] Wang, S., Xie, Y., Niu, S., Lin, L., and Wang, Z. L., "Freestanding triboelectric-layer-based nanogenerators for harvesting energy from a moving object or human motion in contact and non-contact modes," *Advanced Materials* **26**(18), 2818–2824 (2014).

[5] Mallineni, S. S. K., Dong, Y., Behlow, H., Rao, A. M., and Podila, R., "A wireless triboelectric nanogenerator," *Advanced Energy Materials* **8**(10), 1702736 (2018).

[6] Wang, Z. L., Chen, J., and Lin, L., "Progress in triboelectric nanogenerators as a new energy technology and self-powered sensors," *Energy & Environmental Science* **8**(8), 2250–2282 (2015).

[7] Zhu, G., Zhou, Y. S., Bai, P., Meng, X. S., Jing, Q., Chen, J., and Wang, Z. L., "A shape-adaptive thin-film-based approach for 50% high-efficiency energy generation through micro-grating sliding electrification," *Advanced materials* **26**(23), 3788–3796 (2014).

[8] Wang, S., Lin, L., and Wang, Z. L., "Triboelectric nanogenerators as self-powered active sensors," *Nano Energy* **11**, 436–462 (2015).

[9] Chen, J. and Wang, Z. L., "Reviving vibration energy harvesting and self-powered sensing by a triboelectric nanogenerator," *Joule* **1**(3), 480–521 (2017).

[10] Wen, Z., Fu, J., Han, L., Liu, Y., Peng, M., Zheng, L., Zhu, Y., Sun, X., and Zi, Y., "Toward self-powered photodetection enabled by triboelectric nanogenerators," *Journal of Materials Chemistry C* **6**(44), 11893–11902 (2018).

[11] Park, S., Kim, H., Vosgueritchian, M., Cheon, S., Kim, H., Koo, J. H., Kim, T. R., Lee, S., Schwartz, G., Chang, H., et al., "Stretchable energy-harvesting tactile electronic skin capable of differentiating multiple mechanical stimuli modes," *Advanced Materials* **26**(43), 7324–7332 (2014).

[12] Zhang, X.-S., Han, M.-D., Wang, R.-X., Zhu, F.-Y., Li, Z.-H., Wang, W., and Zhang, H.-X., "Frequency-multiplication high-output triboelectric nanogenerator for sustainably powering biomedical microsystems," *Nano letters* **13**(3), 1168–1172 (2013).

[13] Mallineni, S. S. K., Behlow, H., Dong, Y., Bhattacharya, S., Rao, A. M., and Podila, R., "Facile and robust triboelectric nanogenerators assembled using off-the-shelf materials," *Nano Energy* **35**, 263–270 (2017).

[14] Seol, M.-L., Han, J.-W., Moon, D.-I., and Meyyappan, M., "Hysteretic behavior of contact force response in triboelectric nanogenerator," *Nano Energy* **32**, 408–413 (2017).

[15] Niu, S., Wang, S., Lin, L., Liu, Y., Zhou, Y. S., Hu, Y., and Wang, Z. L., "Theoretical study of contact-mode triboelectric nanogenerators as an effective power source," *Energy & Environmental Science* **6**(12), 3576–3583 (2013).

[16] Dharmasena, R. D. I. G., Jayawardena, K., Mills, C., Deane, J., Anguita, J., Dorey, R., and Silva, S., "Triboelectric nanogenerators: providing a fundamental framework," *Energy & Environmental Science* **10**(8), 1801–1811 (2017).

[17] Wen, X., Su, Y., Yang, Y., Zhang, H., and Wang, Z. L., "Applicability of triboelectric generator over a wide range of temperature," *Nano Energy* **4**, 150–156 (2014).

[18] Nguyen, V. and Yang, R., "Effect of humidity and pressure on the triboelectric nanogenerator," *Nano Energy* **2**(5), 604–608 (2013).

[19] Apodaca, M. M., Wesson, P. J., Bishop, K. J., Ratner, M. A., and Grzybowski, B. A., "Contact electrification between identical materials," *Angewandte Chemie International Edition* **49**(5), 946–949 (2010).

[20] Hiratsuka, K. and Hosotani, K., "Effects of friction type and humidity on triboelectrification and triboluminescence among eight kinds of polymers," *Tribology International* **55**, 87–99 (2012).

[21] Zhou, Y. S., Liu, Y., Zhu, G., Lin, Z.-H., Pan, C., Jing, Q., and Wang, Z. L., "In situ quantitative study of nanoscale triboelectrification and patterning," *Nano letters* **13**(6), 2771–2776 (2013).

[22] Watanabe, H., Ghadiri, M., Matsuyama, T., Long Ding, Y., and Pitt, K. G., "New instrument for tribocharge measurement due to single particle impacts," *Review of scientific instruments* **78**(2), 024706 (2007).

[23] Liu, S., Zheng, W., Yang, B., and Tao, X., "Triboelectric charge density of porous and deformable fabrics made from polymer fibers," *Nano energy* **53**, 383–390 (2018).